Linking Stress Drop and Slip Heterogeneity to Assess Source Rupture Directivity for Earthquakes in Central Italy

Cirella A., Calderoni G. & Akinci A.

WP2. Earthquake Source Characteristics and Seismic Wave Propagation in Central Apennines

FINAL MEETING SECURE (DYNAMIC PLANET PROJECT 2023–25)
MARCH 11-12, 2026 – ROME- ITALY

Main Goal

Main Goal

- to improve our knowledge of the relationship between rupture directivity and source complexity;
- to investigate how kinematic/dynamic source heterogeneities may influence stress drop estimates.

To address this goal, we have focused on:

- ✓ linking slip heterogeneity and azimuthal variations of stress drop to assess source rupture directivity effects in near-source region;
- ✓ investigating how stress drop correlates with kinematic rupture properties like rupture velocity and slip asperity , and how it varies along the fault due to source directivity ;
- ✓ answering whether a single stress drop value can describe a spatio-temporal heterogeneous rupture.

Methods

Methods

Kinematic Inversion & 2D Static Stress Changes Algorithms

We retrieve finite-fault slip models from joint inversion of seismic and geodetic data, such as strong motion, high-resolution GPS, and DInSAR measurements (*Cirella et al., 2012* and reference therein). From these models, we compute static stress changes on the fault plane, by using the method proposed by Ripperger and Mai, based on Andrews (1980), which quickly computes static stress variations from slip distributions on a 2D fault plane.

Brune Stress Drop & Directivity Computation

Stress drop was estimated using the Empirical Green's Function (EGF) method in the frequency domain, which isolates source effects by spectral division *(Calderoni et al., 2013, Calderoni & Abercrombie, 2023)*. Corner frequency is computed at each station and inverted to evaluate rupture directivity using a bilateral rupture model.

This framework allows us a direct comparison between spectral parameters and spatial rupture properties.

Case Studies

Case Studies

SECURE
REGIONAL-SCALE EARTHQUAKE GROUND MOTION PREDICTIONS THROUGH PHYSICS-BASED AND EMPIRICAL APPROACHES: A CASE STUDY CENTRAL ITALY

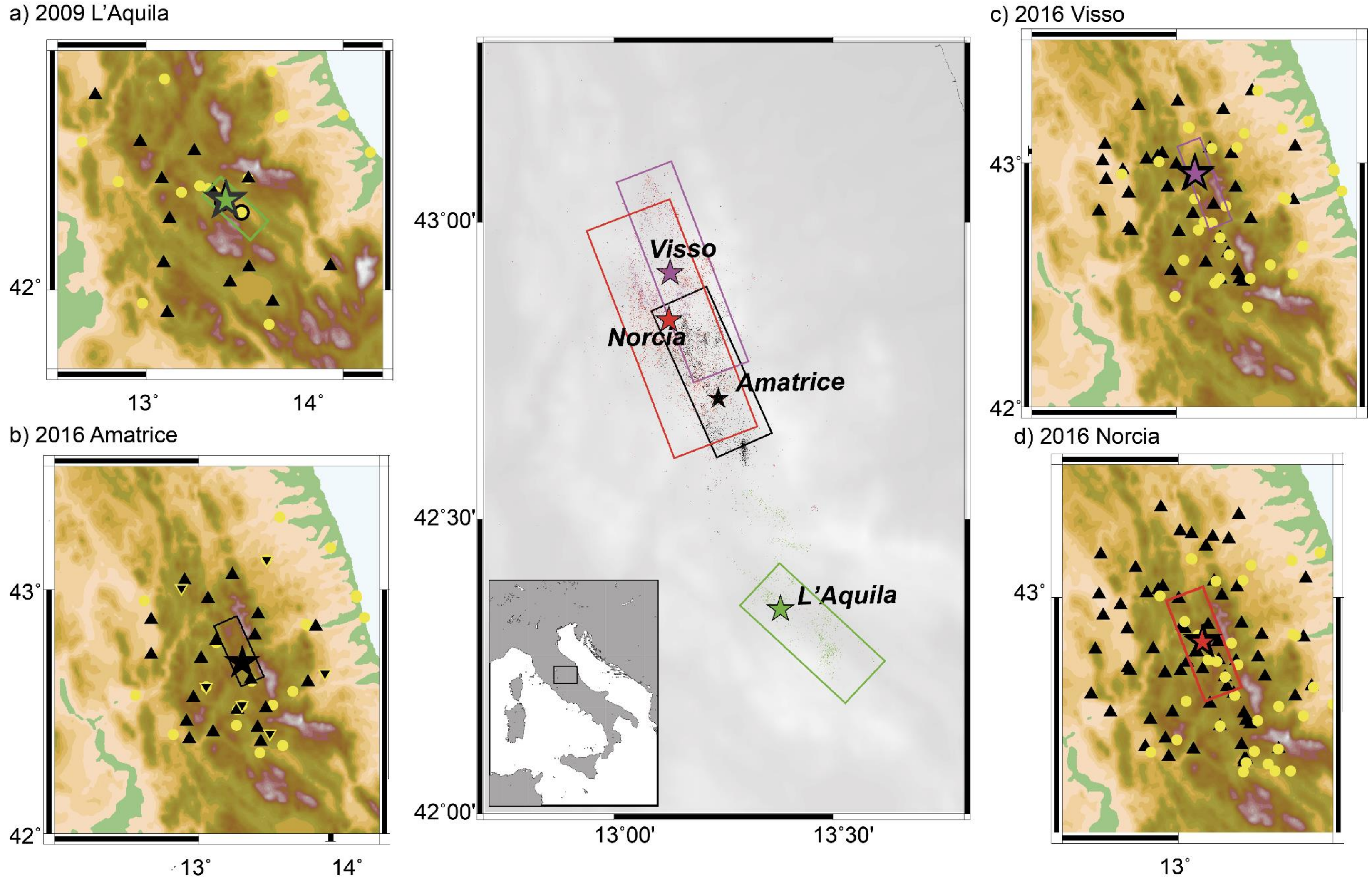

- We analyse data from the 2009 L'Aquila, and the 2016 – 2017 Amatrice – Visso - Norcia (AVN) earthquakes; ideal as they show complex rupture behavior, and strong directivity effects. They also benefit from dense seismic and geodetic datasets, which allow to provide a robust finite-fault modeling.
- For L'Aquila, we use a directivity index between 0 and 1 to measure spectral asymmetry above the corner frequency (*Calderoni et al., 2015*).
- For AVN, a statistical framework based on EGF and a t-test criterion is applied to evaluate spectral ratio differences across station groups oriented forward, backward, and transverse to rupture propagation *(Calderoni et al., 2023).*

Results: 2009 L'Aquila EarthQuake

Results

SR: 8.68 (8.07–9.34)
R = 5.6 km
DIR - SE

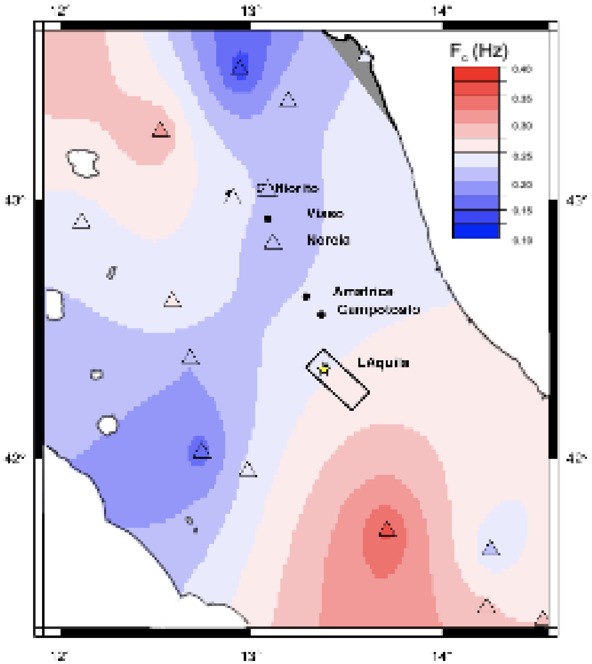

Local Rupture Velocity

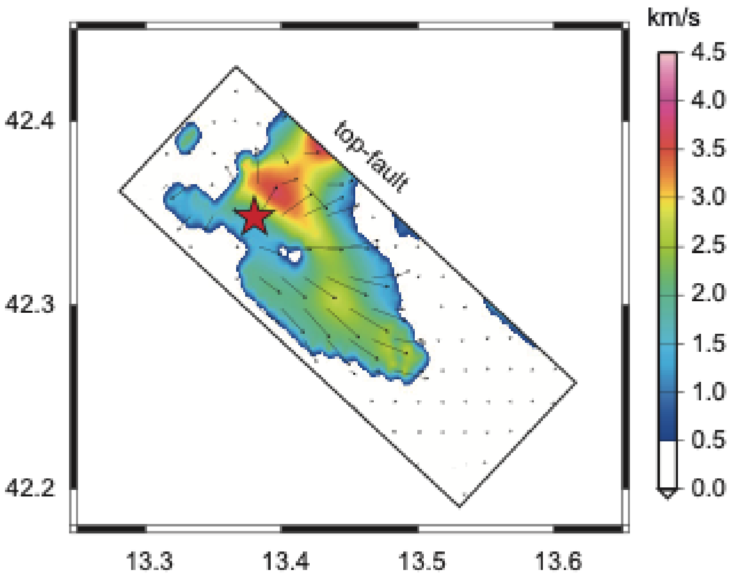

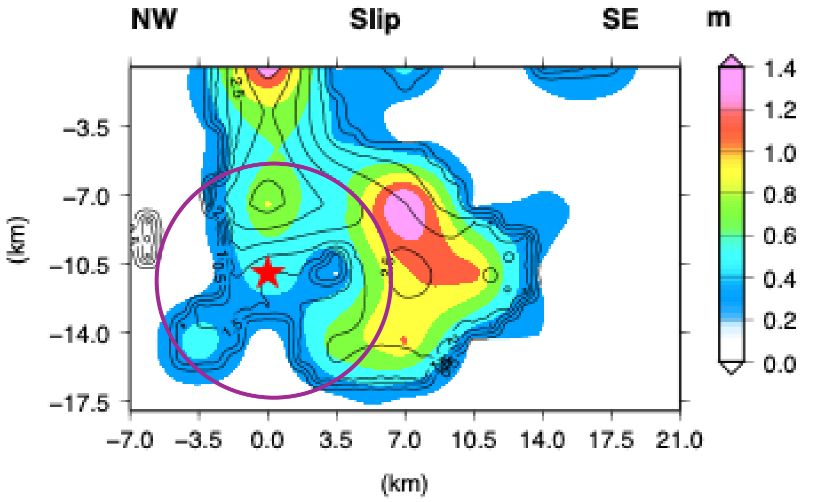

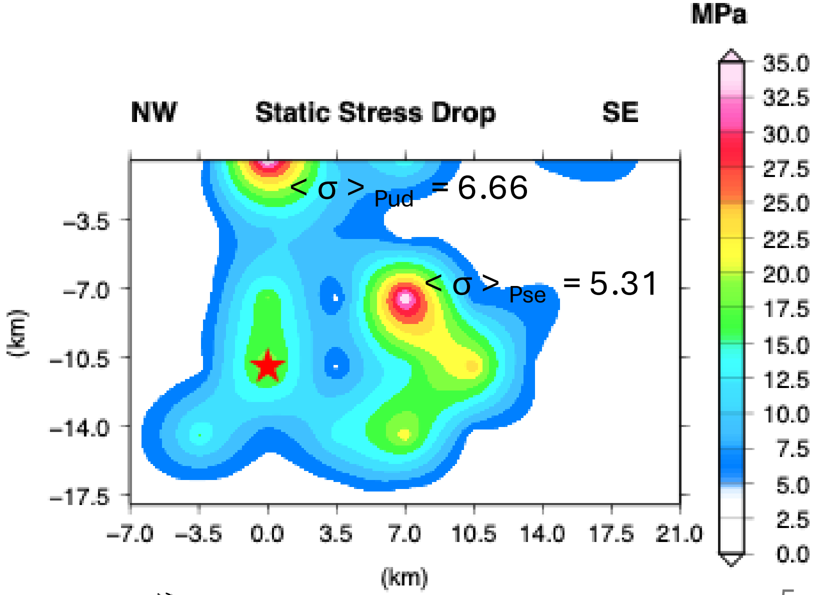

$< \sigma >_{Pud} = 6.66$

$< \sigma >_{Pse} = 5.31$

Δσ=23.4 MPa

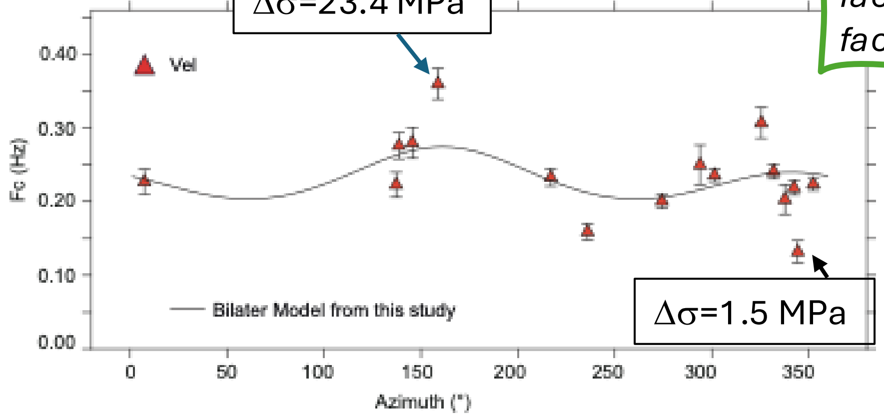

Δσ=1.5 MPa

$fact_{Fc} = 3$
$fact_{Ds} = 20$

$< \sigma > 20\% = 9.79$ MPa

$< \sigma >$of $= 8.92$ MPa

Results: 2016 Amatrice EarthQuake

Results

SECURE
REGIONAL-SCALE EARTHQUAKE GROUND MOTION PREDICTIONS THROUGH PHYSICS-BASED AND EMPIRICAL APPROACHES: A CASE STUDY CENTRAL ITALY

SR: 3.45 (3.18-3.74)
R = 6.2 km
SP: 3.43 (3.29-3.56)
R = 6.2 km
DIR: 325° - 90%

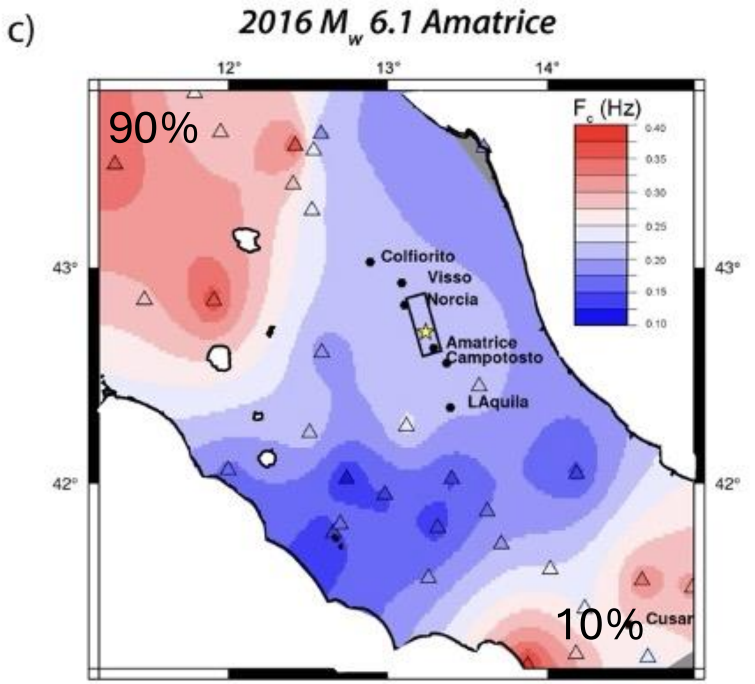

Local Rupture Velocity

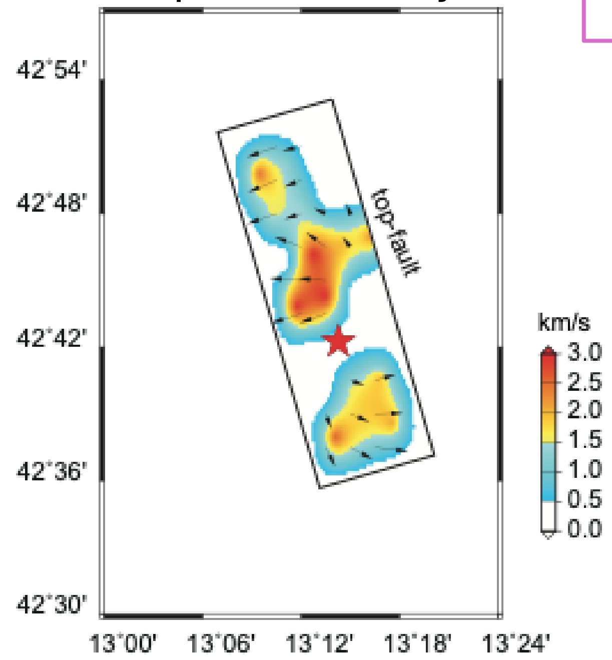

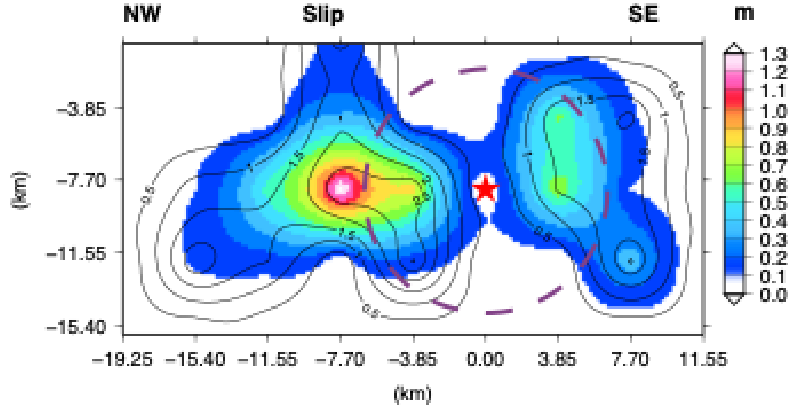

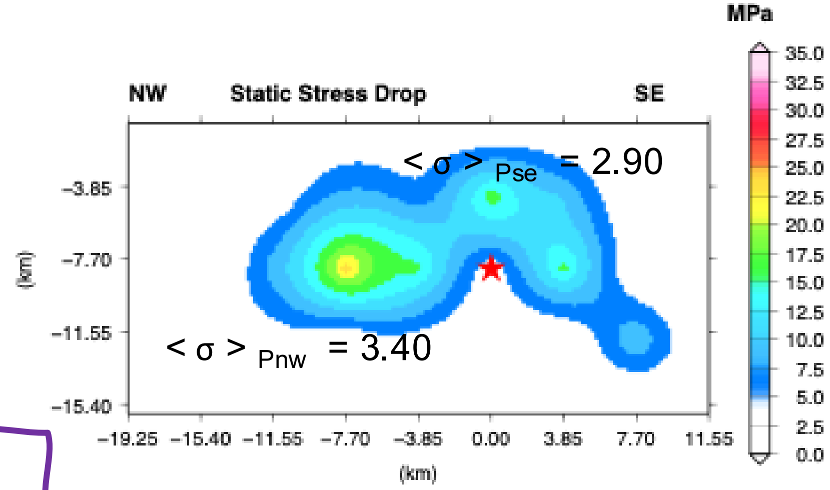

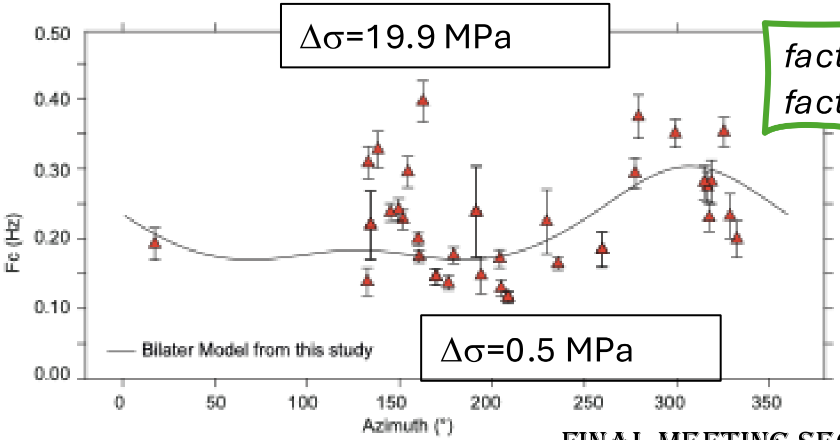

$fact_{Fc}$ = 3
$fact_{\Delta\sigma}$ = 40

< σ > 20% = 7.70 MPa
< σ >of = 7.58 MPa

Results: 2016 Visso EarthQuake

Results

SR: 1.46 (1.42-1.51)
R = 8 km
SP: 2.17 (2.08-2.26)
R = 6.9 km
DIR: 243° - 64%

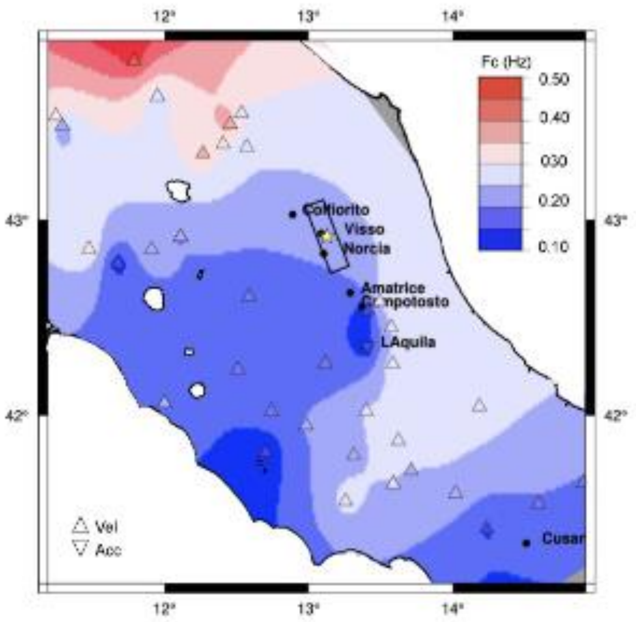

Local Rupture Velocity

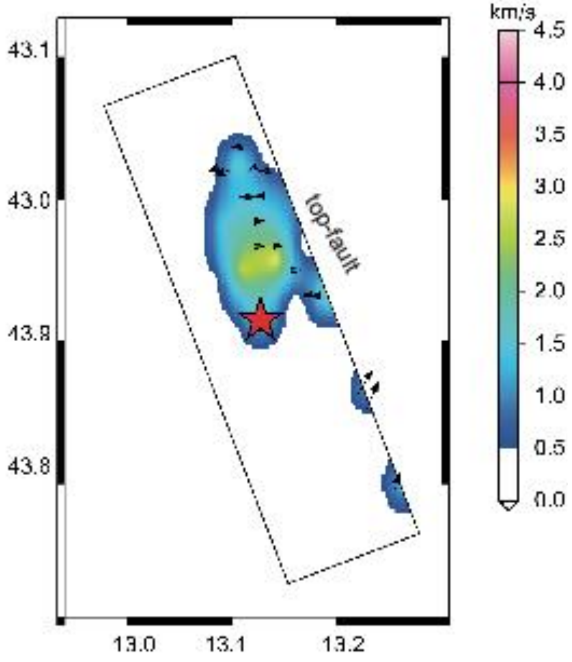

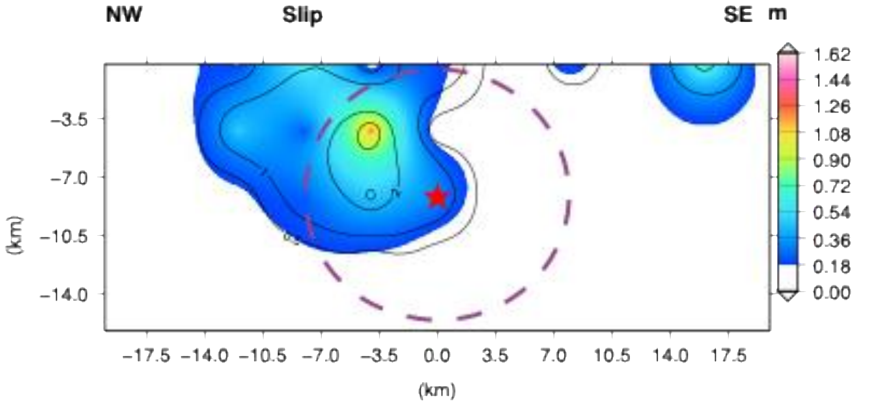

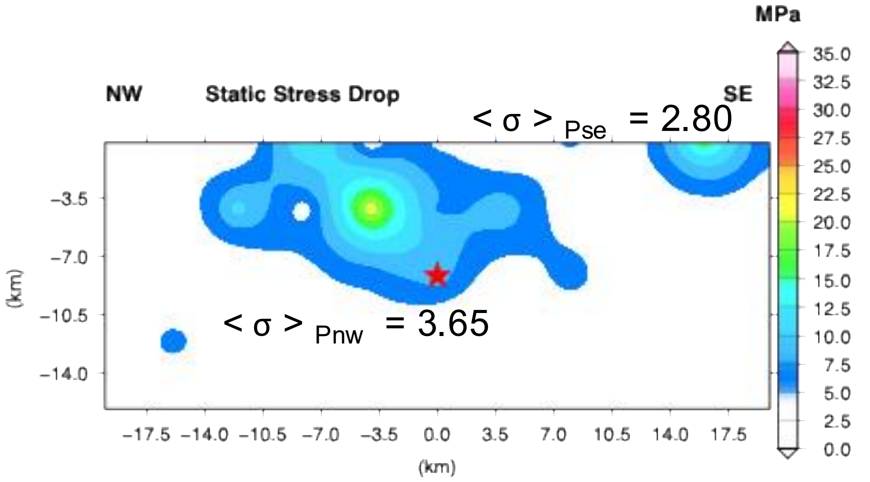

$< \sigma >_{Pse} = 2.80$

$< \sigma >_{Pnw} = 3.65$

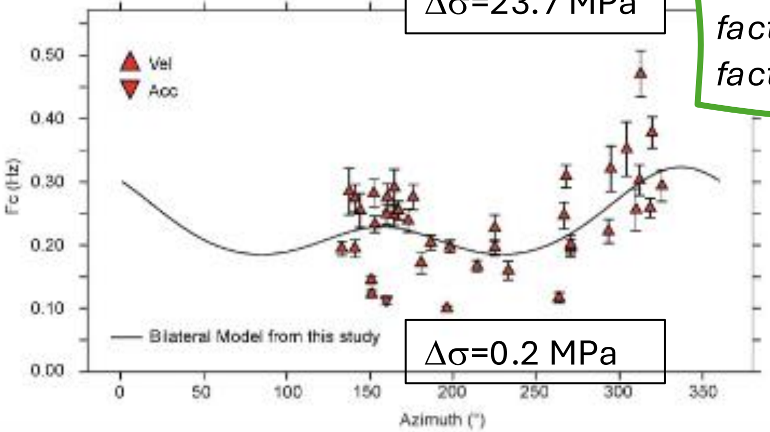

$\Delta\sigma$=23.7 MPa

$\Delta\sigma$=0.2 MPa

$fact_{Fc}$ = 5
$fact_{\Delta\sigma}$ = 100

$< \sigma >_{of}$ = 4.70 MPa
$< \sigma >_{20\%}$ = 5.57 MPa

Results: 2016 Norcia EarthQuake Results

SR: 3.97 (3.70-4.26)
R = 11.4 km
SP: 3.43 (3.27-3.61)
R = 11.3 km
DIR: 196° - 63%

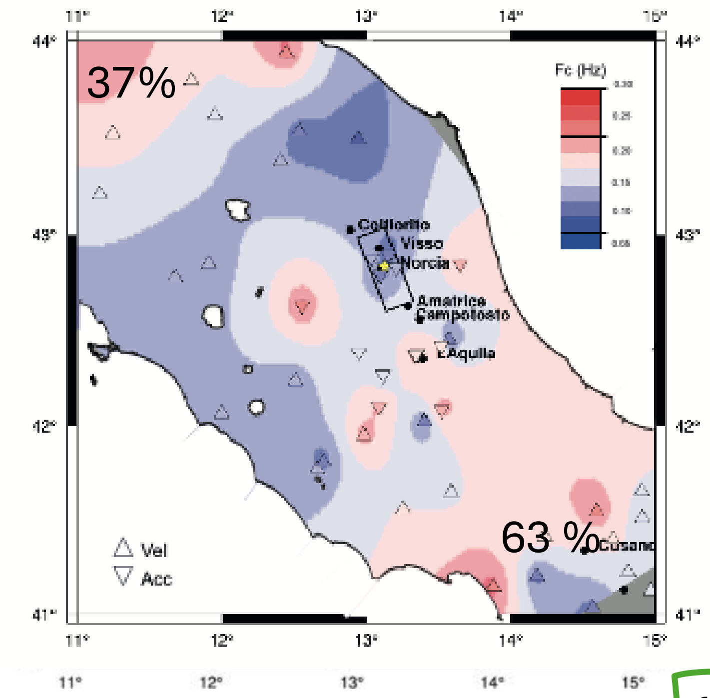

Local Rupture Velocity

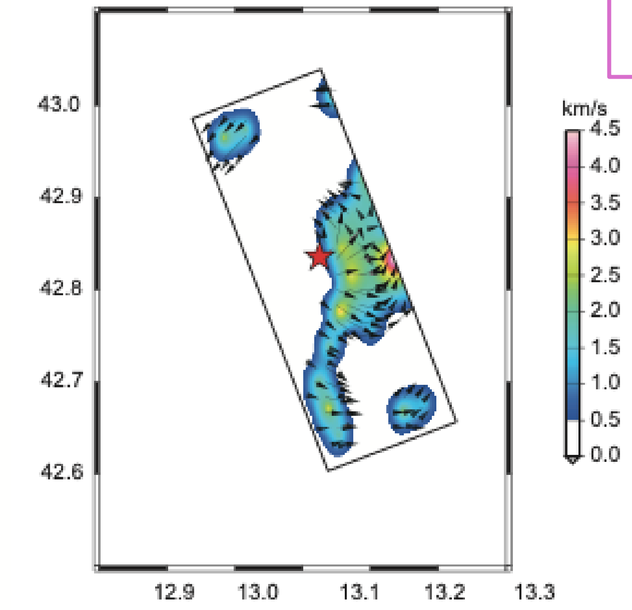

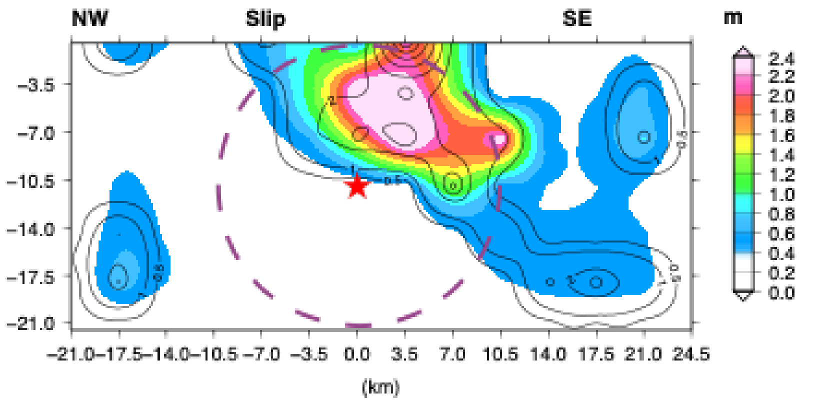

$fact_{Fc}$= 3
$fact_{\Delta\sigma}$ = 17

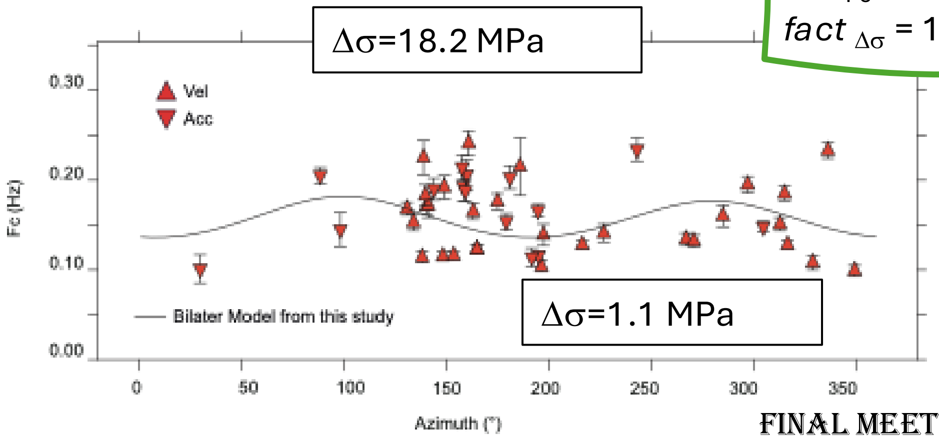

$<\sigma>_{of}$ = 8.38 MPa
$<\sigma>_{20\%}$ = 8.76 MPa

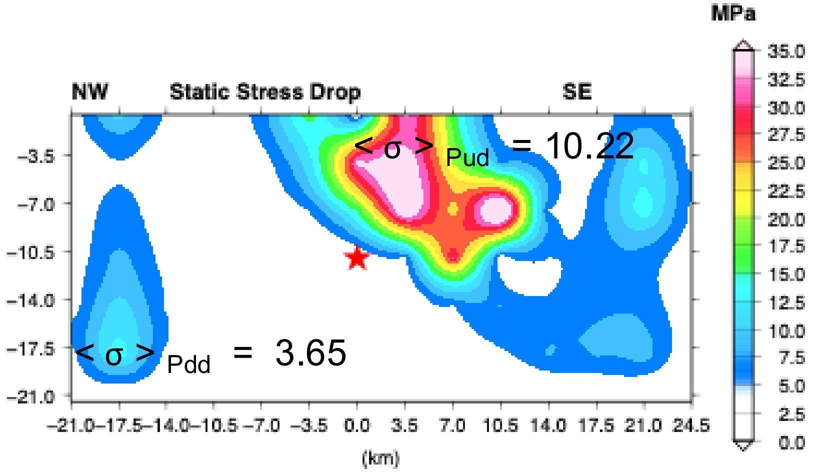

Brune Stress Drop Comparison & On-Fault Stress Drop Estimate (this Study)

REGIONAL-SCALE EARTHQUAKE GROUND MOTION PREDICTIONS THROUGH PYHSICS-BASED AND EMPIRICAL APPROACHES: A CASE STUDY CENTRAL ITALY

Mainshock	*Δσ (MPa)*	*2D Static Stress Changes (MPa)*	*Δσ (MPa) Other studies*	
M_w6.1 L'Aquila	SR: 8.68 (8.07–9.34) R = 5.6 km DIR - SE Calderoni et al., 2019	$<\sigma>_{of}$ = 8.92 $<\sigma>_{Pse}$ = 5.31 $<\sigma>_{Pud}$ = 6.66 $<\sigma>_{20\%}$ = 9.79	Ameri et al., (2011) Bindi et al. (2009-2011): Malagnini et al. (2011): Ameri et al., (2012): Calderoni et al., (2013) Pacor et al. (2016):	60 9.2 15 10 10 25
M_w6.1 Amatrice	SR: 3.45 (3.18-3.74) R = 6.2 km SP: 3.43 (3.29-3.56) R = 6.2 km DIR: 325° - 90% Calderoni et al., 2023a-b	$<\sigma>_{of}$ = 7.58 $<\sigma>_{Pse}$ = 2.90 $<\sigma>_{Pnw}$ = 3.40 $<\sigma>_{20\%}$ = 7.70	**Gallovič et al. (2019) Morasca et al., (2019) Bindi et al., (2020) Kemna et al., (2021): Morasca et al., (2022) CCT: GIT:	4 10 23 2.7 3.96 4.67
M_w5.9 Visso	SR: 1.46 (1.42-1.51) R = 8 km SP: 2.17 (2.08-2.26) R = 6.9 km DIR: 243° - 64% Calderoni et al., 2023a-b	$<\sigma>_{of}$ = 4.70 $<\sigma>_{Pse}$ = 2.80 $<\sigma>_{Pnw}$ = 3.65 $<\sigma>_{20\%}$ = 5.57	Kemna et al., (2021): Morasca et al., (2022) CCT: GIT:	2.6 3.78 3.57
M_w6.3 Norcia	SR: 3.97 (3.70-4.26) R = 11.4 km SP: 3.43 (3.27-3.61) R = 11.3 km DIR: 196° - 63% Calderoni et al., 2023a-b	$<\sigma>_{of}$ = 8.38 $<\sigma>_{Pdd}$ = 3.65 $<\sigma>_{Pud}$ = 10.22 $<\sigma>_{20\%}$ = 8.76	Bindi et al., (2020) **Tinti et al. (2021) Kemna et al., (2021): Morasca et al., (2022) CCT: GIT:	20 2–4 2.5 3.88 5.52

Mainshock		M_w	Δσ (MPa)	V_r/β	*k*	RMS	Azi (°)
L'Aquila	2009-04-06 01:32	6.1	8.68	0.38	0.55	0.20	161
Amatrice	2016-08-24 01:36	6.1	3.45	0.39	0.31	0.18	306
Visso	2016-10-26 19:18	5.9	1.46	0.49	0.39	0.12	337
Norcia	2016-10-30 06:40	6.3	3.97	0.42	0.51	0.11	100

SR: : Brune stress drop from Spectral Ratio
SP: : Brune stress drop from Spectral Fitting
*$<\sigma>_{20\%}$: mean stress changes (> 20% average slip)
*$<\sigma>_{of}$: mean stress changes over all fault distribution
*$<\sigma>_{P}$: mean stress changes computed on a single patch
**. : mean stress drop from dynamic rupture model
CCT : Brune stress drop from Coda Calibration Technique
GIT : Brune stress drop from non-parametric inversion of source, attenuation, and site

Conclusion

Key Take Aways

Across all events analysed, several consistent patterns emerge:

- large-slip asperities are systematically associated with elevated static stress drop;
- the location and strength of slip asperities relative to the nucleation point play a key role in controlling rupture directivity and velocity, which in turn govern the azimuthal variation of corner frequency and contribute to large uncertainties in the stress drop parameter;
- all the static stress drop patterns computed from the inverted earthquake slip distribution highlight strong heterogeneity in the stress redistribution and directional high-frequency radiation due to the source rupture complexity.
- the estimated stress drop values are generally higher near the fault compared to those derived from spatially averaged datasets, likely reflecting the limitations of the Brune point-source approximation when applied to finite–fault ruptures;

Implications

Take Home Message

SECURE
REGIONAL-SCALE EARTHQUAKE GROUND MOTION PREDICTIONS THROUGH PYHSICS-BASED AND EMPIRICAL APPROACHES: A CASE STUDY CENTRAL ITALY

- Heterogeneous stress drop distributions enhance forward rupture amplification, which primarily governs the observed azimuthal variability in high-frequency ground motions. This variability can be extreme—for example, in the 2016 Amatrice mainshock, corner frequency varied by up to a factor of 40 between forward and backward directions— **making single-value stress drop estimates inherently unreliable.**

Implications:

- ✓ Estimating a single stress drop value is neither straightforward nor reliable; worthy of noting that it is essential to treat stress drop as a parameter that varies in both space and time.
- ✓ The integrated approach adopted in this study—combining EGF-based stress drop estimates with finite–fault kinematic inversions—provides a robust framework for advancing our understanding of rupture dynamics, slip heterogeneity, stress transfer and the spatial variability of stress drop.

Take Home Message

- ❑ Our results emphasise the importance of accounting for source complexity in near-fault seismic hazard characterisation, where complex source effects play a major role.

- ❑ Such insights are crucial for developing next-generation ground motion prediction models; for improving seismic hazard assessments and informing future risk mitigation strategies in seismically active region, as the Central Italy.

Thank For Your Attention

Thank For Your Suggestion

Calderoni,G., A. Cirella, and A. Akinci, 2026.
“ *Linking Stress Drop and Slip Heterogeneity to Assess Source Rupture Directivity for Earthquakes in Central Italy.*”
Terra Nova 1–10. https://doi.org/10.1111/ter.70026.

References

References

Andrews, D. J. (1980), A stochastic fault model: 1. Static case, J. Geophys. Res., 85, 3867–3877.

Calderoni, G., A. Rovelli, and S. K. Singh (2013). Stress drop and source scaling of the 2009 April L'Aquila earthquakes, Geophys. J. Int. 192, no. 1, 260–274, doi: 10.1093/gji/ggs011.

Calderoni, G., Rovelli, A., Ben-Zion, Y., & Di Giovambattista, R. (2015). Along-strike rupture directivity of earthquakes of the 2009 L'Aquila, central Italy, seismic sequence. Geophysical Journal International, 203(1), 399–415. https://doi.org/10.1093/gji/ggv275

Calderoni & Abercrombie 2023,

Calderoni, G., R. Di Giovambattista, and G. Ventura. 2023. "A Reliable Procedure to Estimate the Rupture Propagation Directions from Source Directivity: The 2016–2018 Central Italy Seismic Sequence." Seismological Research Letters: 1–13. https:// doi. org/ 10. 1785/ 02202 20318 .

Cirella A., Piatanesi A., Tinti E. Chini M. and M. Cocco, (2012), "Complexity of the rupture process during the 2009 L'Aquila, Italy, earthquake", Geophysical Journal International, 190, 607-621, doi:10.1111/j.1365-246X.2012.05505.x

Guatteri, M., P. M. Mai, and G. C. Beroza (2004), A Pseudo-Dynamic Approximation to Dynamic Rupture Models for Strong Ground Motion Prediction. *Bulletin of the Seismological Society of America* 2004; 94 (6): 2051–2063. doi: https://doi.org/10.1785/0120040037

Ripperger, J., and P. M. Mai (2004), Fast computation of static stress changes on 2D faults from final slip distributions, *Geophys. Res. Lett.*, 31, L18610, doi:10.1029/2004GL020594

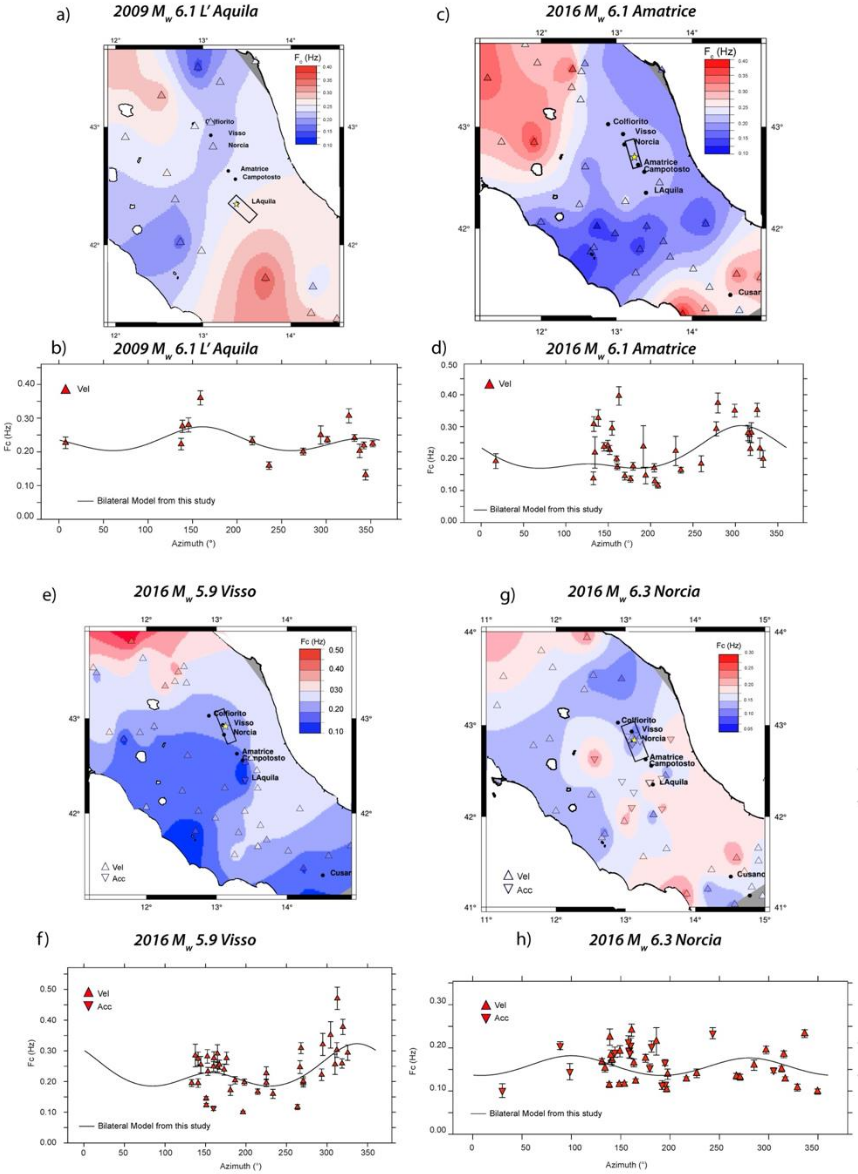

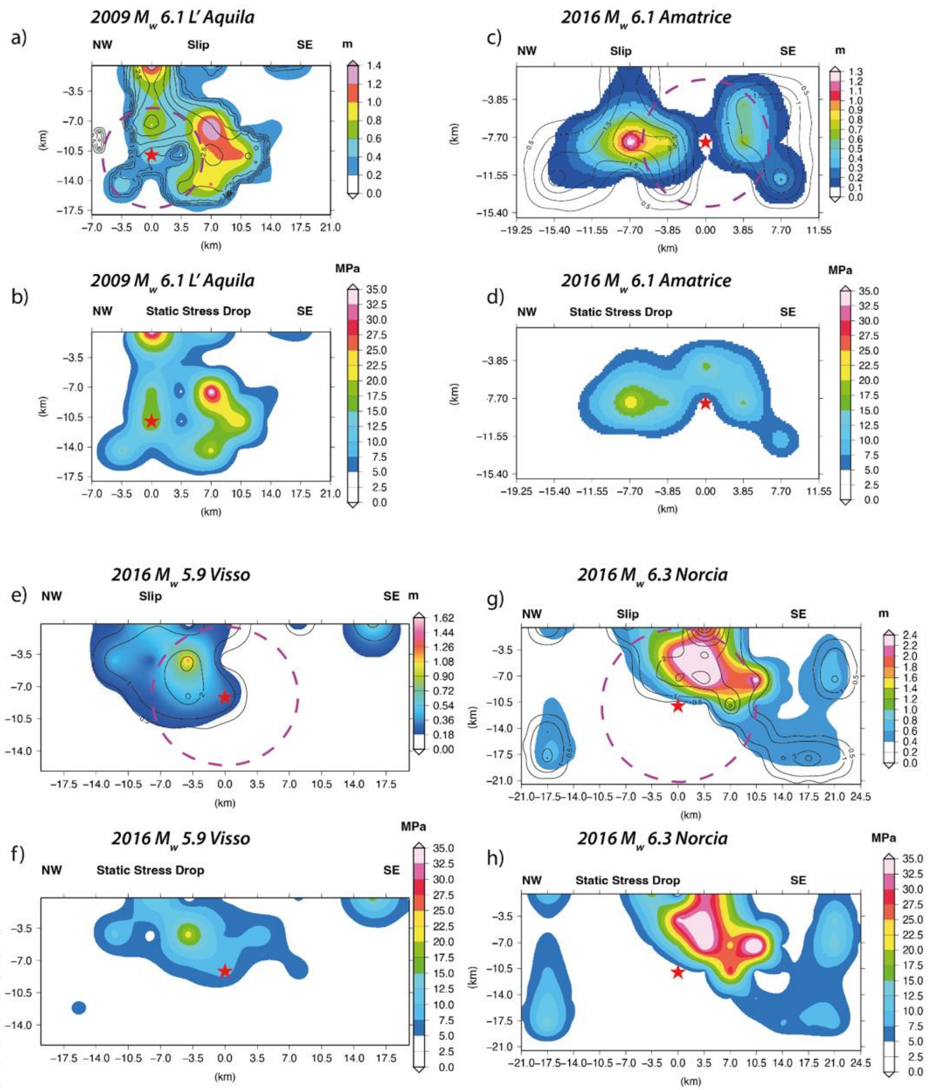

Local Rupture Velocity

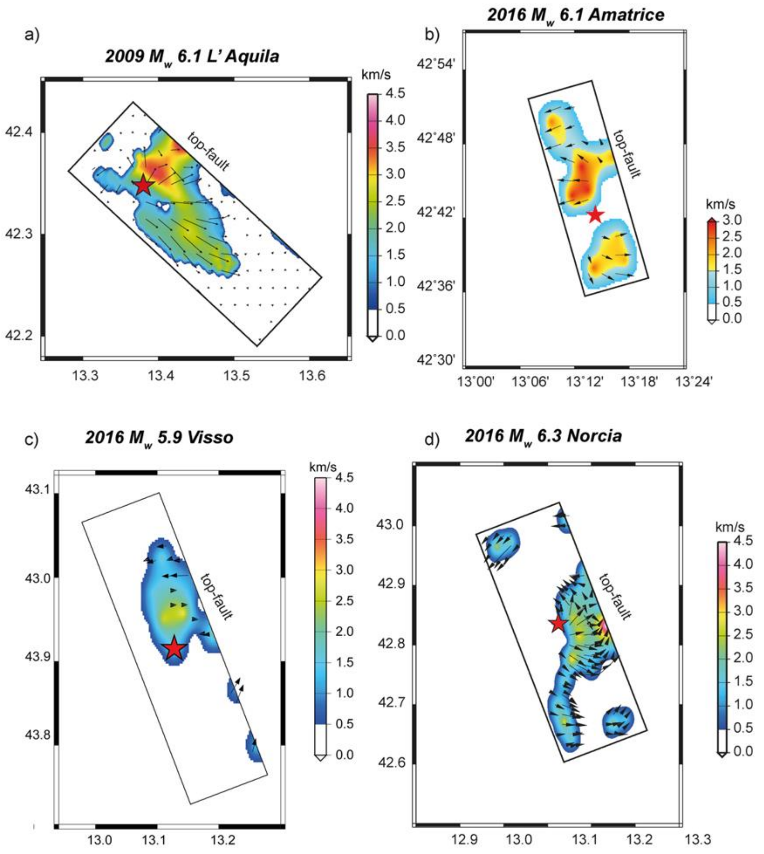

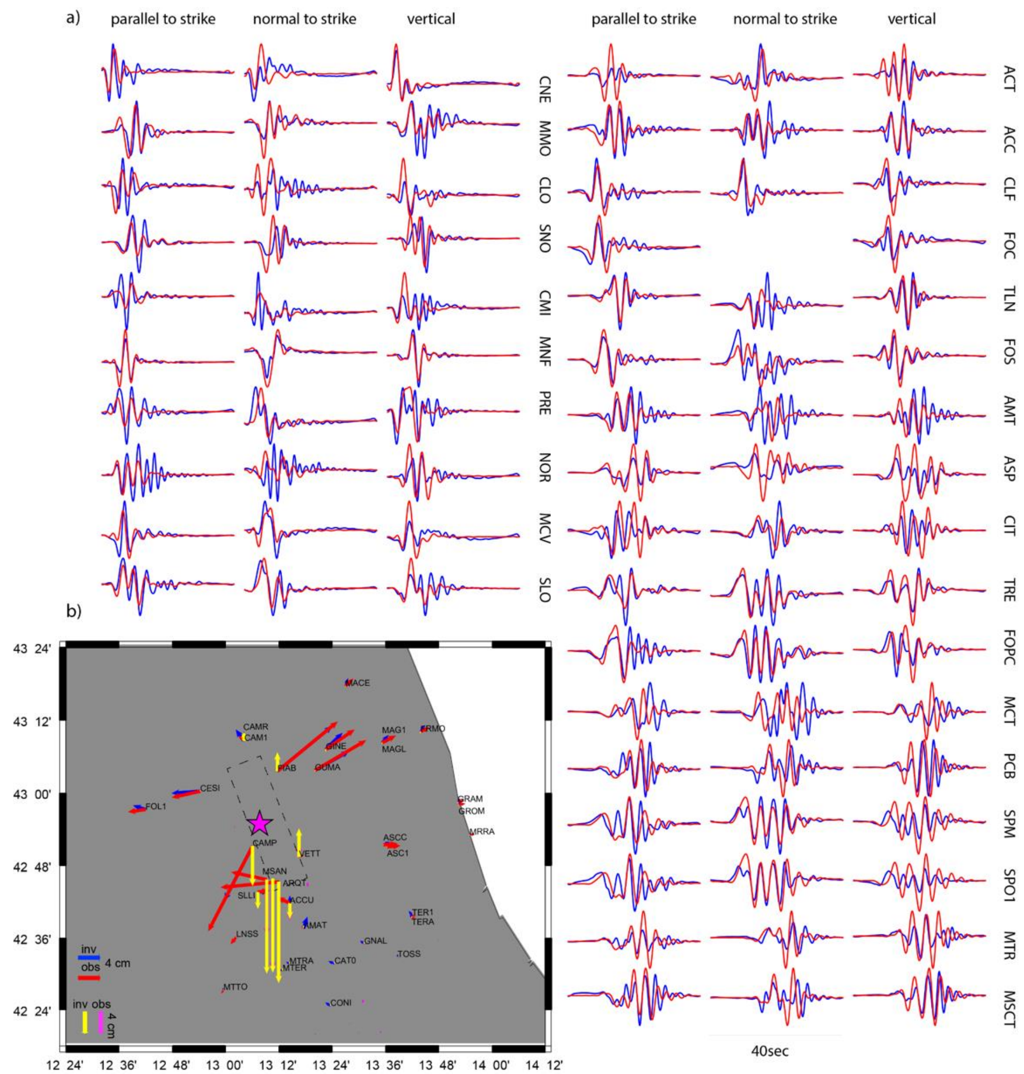

The 2016 Visso Earthquake. Dataset misfit:

(a) Comparison of recorded strong motion (blue lines) with synthetic waveforms (red lines).

(b) Comparison of measured (red and pink arrows) with synthetic (blue and yellow arrows) horizontal and vertical (respectively) coseismic displacements.

The 2016 Norcia Earthquake. (a) Comparison of recorded strong motion (blue lines) with synthetic (red lines); (b) Comparison of measured (red and pink arrows) with synthetic (blue and yellow arrows) horizontal and vertical (respectively) coseismic displacements.

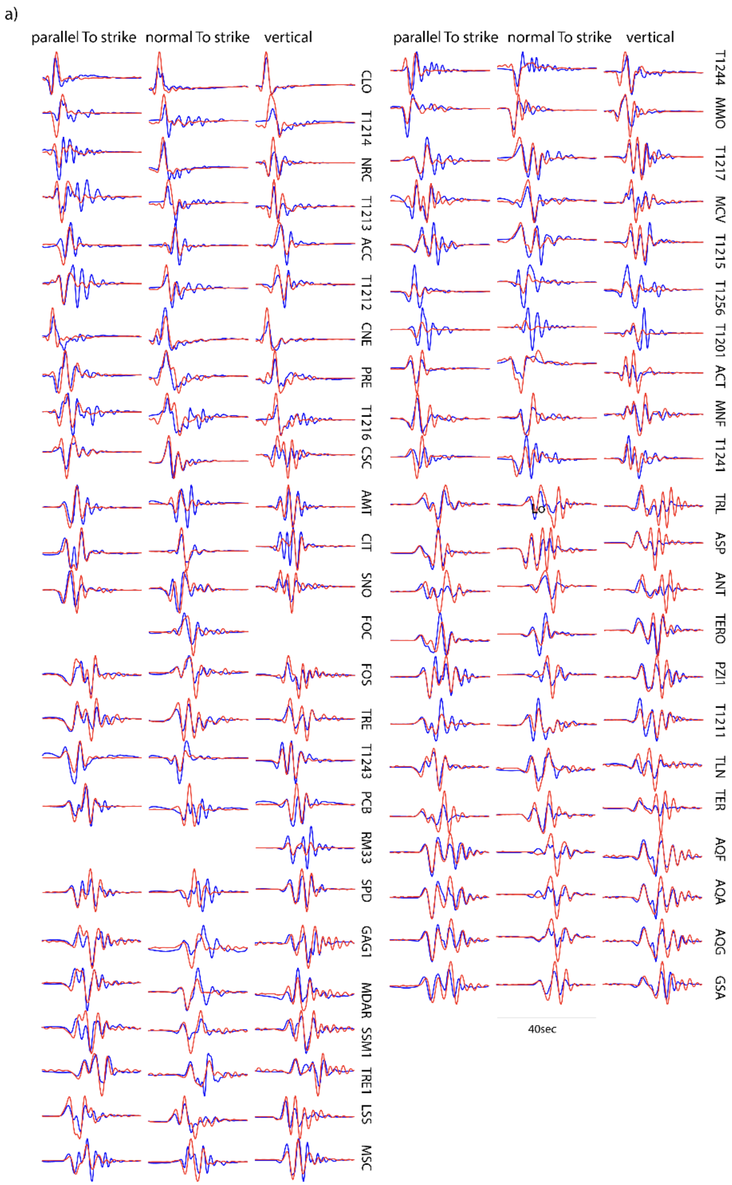

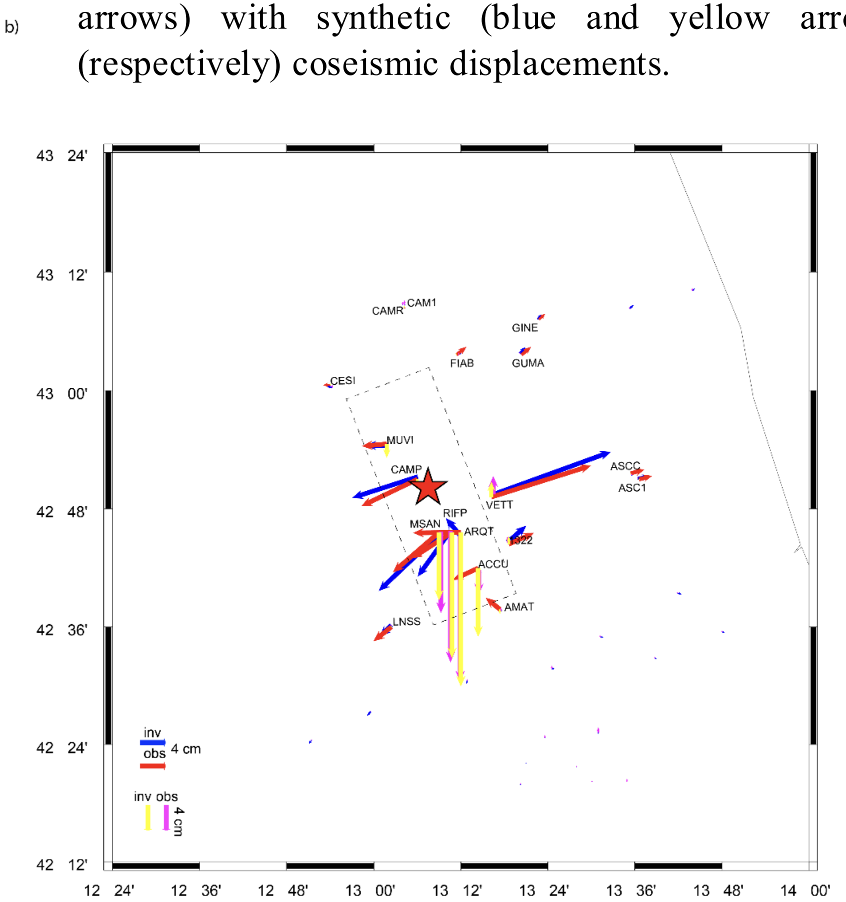

The 2016 Norcia Earthquake. Observed, synthetic DInSAR displacements and their residuals (left, central, and right, panels, respectively), recorded by ascending ALOS-2 (upper panels), and descending SENT-1 (bottom panels) satellites. Geodetic dataset is taken from Cheloni et al. (2019). Black dashed box represents the surface projection of the fault plane. Black contour lines display the retrieved slip model.

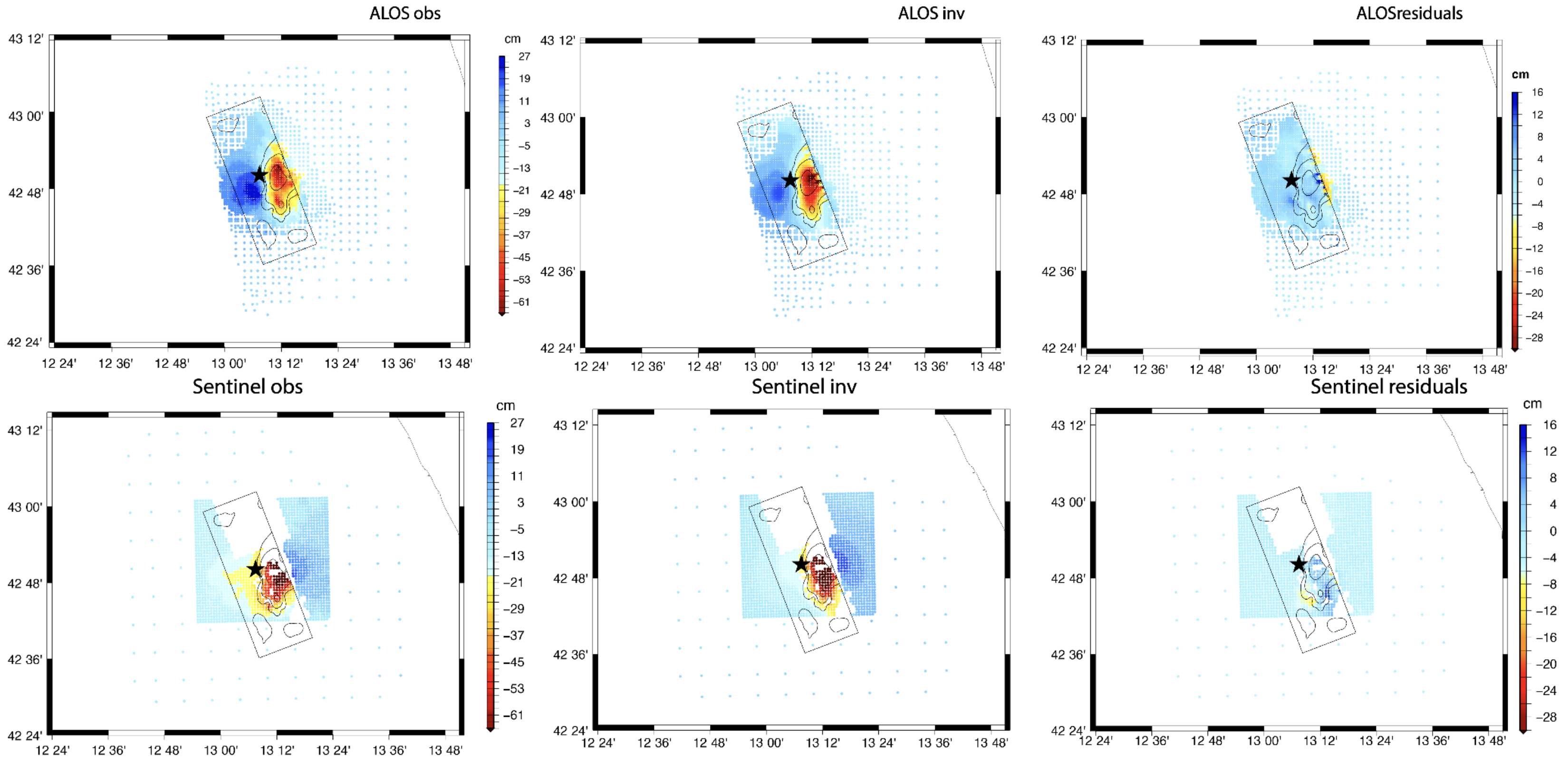

Supplementary Material

Brune Stress Drop & Directivity Computation

Understanding rupture propagation is essential for evaluating the azimuthal distribution of ground shaking and related seismic hazards. In this study, we used Target–EGF pairs from Calderoni et al. (2015) and (2023) for the AQU and AVN sequences, respectively. For each station, we calculated the mean corner frequency using these pairs, based on equations linking corner frequency to stress drop estimated via the EGF method (Keilis-Borok, 1959; Eshelby, 1957).

$$\Delta\sigma = \frac{7}{16}\frac{M_0}{r}$$

$$r = \frac{0.3724\,\beta}{f_0}$$

Here, r denotes the radius of a circular crack in an infinite Poissonian medium, and Δσ is the uniform stress drop. We inverted the target-event corner frequencies across stations using a bilateral rupture model (Ben-Menahem, 1961). Assuming a homogeneous kinematic bilateral line-source, rupture directivity influences spectral amplitude, scaled by the directivity coefficient Cnd. The exponent n reflects the source model: n = 2 for an omega-squared model with a single corner frequency, and n = 1 for models with two corner frequencies. We adopt n = 2, consistent with the single-corner omega-squared model.

Supplementary Material

Brune Stress Drop & Directivity Computation

$$C_d = \left(\frac{k^2}{(1 - \frac{v_r}{\beta}\cos\vartheta)^2} + \frac{(1-k)^2}{(1 + \frac{v_r}{\beta}\cos\vartheta)^2} \right)^{1/2}$$

The parameter k denotes the fraction of rupture length propagating in direction φ, identifying the predominant rupture direction when $k > 0.5$. If $k < 0.5$, rupture mainly propagates toward φ ± 180°. For symmetric bilateral rupture at constant velocity, the corner frequency fc relates to the directivity coefficient as fc = Cd vr / L, with the shortest source duration in the rupture direction. Following Calderoni et al. (2020), we assumed a constant rupture velocity to examine corner frequency (or stress drop) variability rather than absolute values.

Supplementary Material

Global search inversion technique for moderate to great earthquakes

Planar

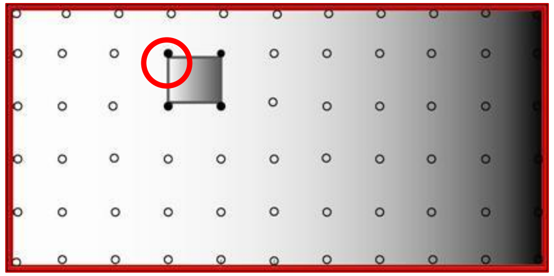

Non-planar

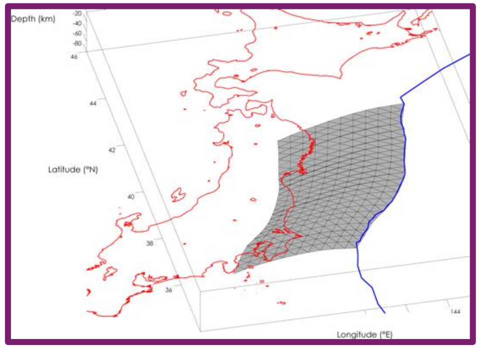

Inversion parametrization/approach

- planar, **non-planar fault surface**;
- finite fault is divided into subfaults;
- different crustal models (1D, 3D);
- **kinematic parameters are allowed to vary within a subfault**;
- **different forward numerical modeling depending on the kind of data (DW/FE,FD);**
- model spatial resolution depends on data frequency content.

Inverted parameters

- Slip;
- **Rise Time;**
- Rupture Time;
- Rake;
- **Peak Slip Velocity**.

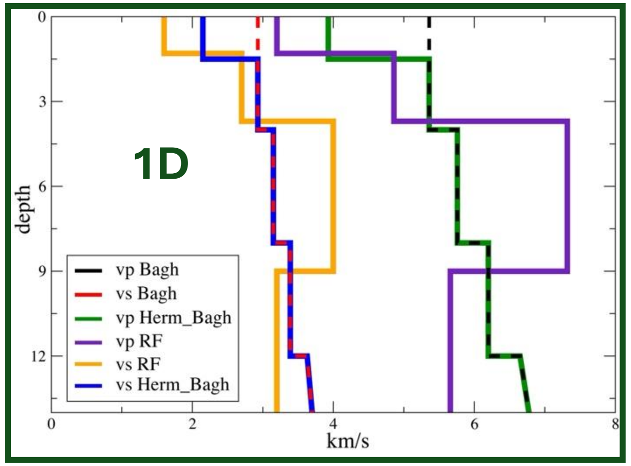

3D velocity models

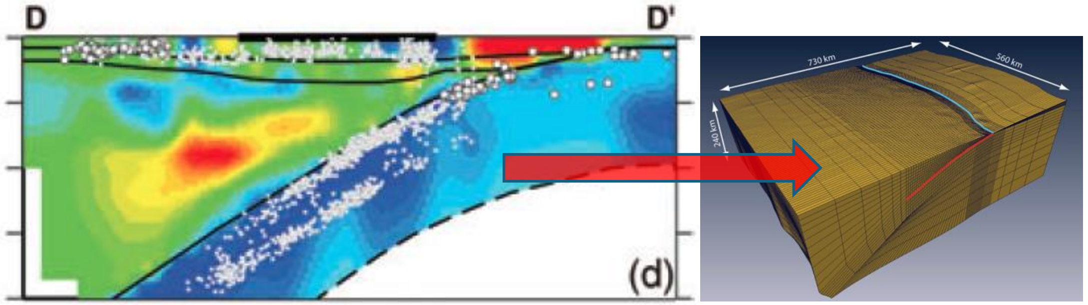

Seismic tomography, Huang et al., 2011

Global search inversion technique for moderate to great earthquakes

Step-1: Heat-Bath Simulated Annealing

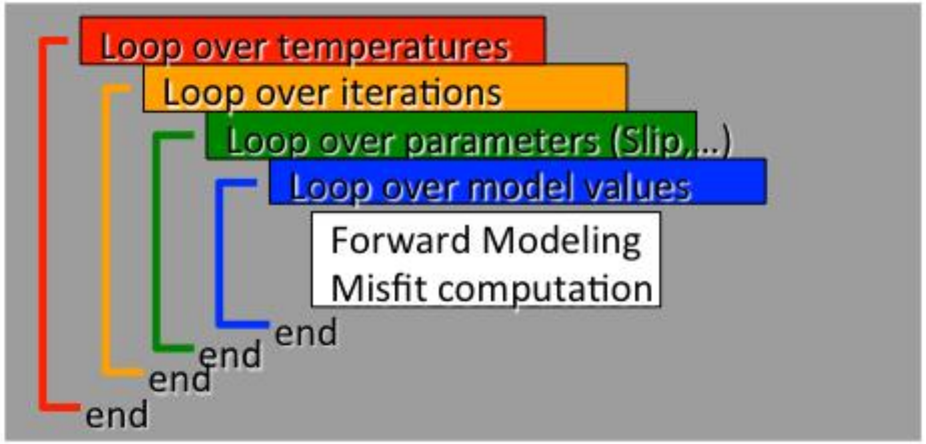

ADVANTAGES

- capability to solve non linear problems with a huge number of parameters;
- efficient model space exploration;
- reduced probability to remain entrapped in a local minimum;
- huge number of explored models (~1M)

MAIN LIMIT

- computationally expensive.

Step-2: Ensemble Appraisal

Output of kinematic inversion:

- Model Ensemble Ω = Rupture Models (m) & Cost Function C(m)

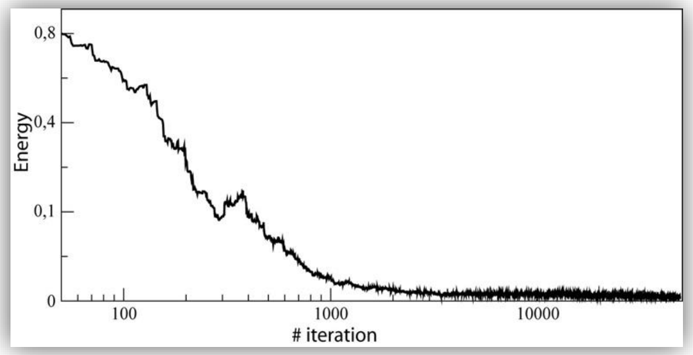

- **Best Model**
- Average Model (median, mode)

$$\langle m_i \rangle = \frac{\sum_{j \in \Omega} m_{ij}/E_j}{\sum_{j \in \Omega} 1/E_j}$$

- Standard Deviation

$$\langle \sigma_i \rangle^2 = \frac{\sum_{j \in \Omega} [m_{ij} - \langle m_i \rangle]^2 / E_j}{\sum_{j \in \Omega} 1/E_j}$$

Supplementary Material

Kinematic parameter ranges' variability adopted to invert for each earthquake source model.

	Peak Slip Velocity [m/s]	Rise Time [s]	Rupture Velocity [km/s]	Rake [°]
L'Aquila	0 – 3.5	0.75 – 3.00	1.4 – 4.0	230 - 310
Amatrice	0 – 3.5	0.75 – 3.00	1.4 – 4.0	-115 - -55
Visso	0 – 2.5	0.75 – 2.50	1.5 – 3.0	-113 - -73
Norcia	0 – 5.0	0.75 – 4.00	1.4 – 4.0	-110 - -70

Fast computation of static stress changes on 2D faults from final slip distributions

Computing the distribution of static stress changes on the fault plane of an earthquake, given the distribution of static displacements, is of great importance in earthquake dynamics. The static stress change on the fault plane itself is linked to the dynamics of earthquake rupture and hence also to the associated energy release and seismic radiation. Its knowledge is therefore required in dynamic rupture modeling of past (and future) earthquakes [Peyrat et al., 2001]. Moreover, stress-drop distributions for simu- lated slip maps in scenario earthquakes for near-source strong-motion simulations allow to constrain the temporal rupture evolution [Guatteri et al., 2003] and the energy budget of earthquake rupture [Guatteri et al., 2004]

This method extends the approach developed by Andrews [1980], a wave number representation relating the distribution of static slip to the associated collinear static stress change, in order to account for both slip-parallel and slip-perpendicular stress changes.

One of the fundamental quantities in earthquake source physics is the static stress change associated with earthquake faulting. The static stress change on the fault plane itself is linked to the dynamics of earthquake rupture and hence also to the associated energy release and seismic radiation. The purpose is to constrain dynamic rupture models and **construct physically consistent source characterizations for strong-motion simulations**

Fast computation of static stress changes on 2D faults from final slip distributions
Ripperger & Mai, 2004

2. Method

2.1. Description

[6] For a given slip distribution $D(\mathbf{x})$ on a planar fault, *Andrews* [1974] presented the following expressions for the two components (parallel and perpendicular to the slip direction), of shear strain on the fault:

$$\varepsilon_{\parallel}(\mathbf{x}) = \frac{1}{8\pi} \iint \frac{1}{r} \left[\frac{2(\lambda+\mu)}{\lambda+2\mu} \frac{\partial^2 D(\mathbf{x})}{\partial x_{\parallel}^2} + \frac{\partial^2 D(\mathbf{x})}{\partial x_{\perp}^2} \right] dx_{\parallel} dx_{\perp} \quad (1)$$

$$\varepsilon_{\perp}(\mathbf{x}) = \frac{1}{8\pi} \iint \frac{1}{r} \left[\frac{2(\lambda+\mu)}{\lambda+2\mu} - 1 \right] \frac{\partial^2 D(\mathbf{x})}{\partial x_{\parallel} \partial x_{\perp}} dx_{\parallel} dx_{\perp} \quad (2)$$

Based on equation (1), *Andrews* [1978, 1980] developed a formulation which relates the slip-parallel shear-stress change to the slip distribution in the wave number domain:

$$\Delta\sigma_{\parallel}(\mathbf{k}) = K_{\parallel}(\mathbf{k}) D(\mathbf{k}) \quad (3)$$

Here, written as functions of the wave number vector $\mathbf{k}$, D is the static slip distribution, $\Delta\sigma_{\parallel}$ is the component of shear-stress change parallel to the slip direction and $K_{\parallel}$ is the static stiffness matrix given by

$$K_{\parallel}(\mathbf{k}) = -\frac{1}{2} \frac{\mu}{\sqrt{k_{\parallel}^2 + k_{\perp}^2}} \left[\frac{2(\lambda+\mu)}{\lambda+2\mu} k_{\parallel}^2 + k_{\perp}^2 \right], \quad (4)$$

with $k_{\parallel}$ and $k_{\perp}$ being the wave numbers in the directions parallel and perpendicular to the slip direction, respectively, and λ and μ being the Lamé constants. Starting from equation (2) and proceeding in an analogous manner, we derive a similar expression for the component of shear-stress change perpendicular to the slip direction:

$$\Delta\sigma_{\perp}(\mathbf{k}) = K_{\perp}(\mathbf{k}) D(\mathbf{k}), \quad (5)$$

where the slip-perpendicular static stiffness function is given by

$$K_{\perp}(\mathbf{k}) = -\frac{1}{2} \frac{\mu}{\sqrt{k_{\parallel}^2 + k_{\perp}^2}} \left[\frac{2(\lambda+\mu)}{\lambda+2\mu} - 1 \right] k_{\parallel} k_{\perp}. \quad (6)$$

Calculating the static stress changes for a given slip distribution therefore only requires the Fourier transformation of slip into the wave number domain, application of equations (3) and (5) and the inverse transformation of $\Delta\sigma(\mathbf{k})$ back into space domain. Varying rake angles are

A general problem in calculating stress changes from slip arises if non-zero slip occurs at the edges of the fault plane. Non-zero slip at the fault boundaries constitutes a discontinuity in slip that will always lead to unrealistically high values of stress change at the edges.

Supplementary Material

Directivity parameters obtained using bilateral rupture model.

Mainshock	M_w	$\Delta\sigma$ (MPa)	V_r/β	*k*	Sdv	Azi (°)
L'Aquila	6.1	8.65	0.38	0.55	0.20	161
Amatrice	6.0	3.45	0.39	0.31	0.18	306
Visso	5.9	1.46	0.49	0.38	0.12	330
Norcia	6.3	3.97	0.41	0.51	0.10	141

Hyopcentral Local Rupture Velocity

	Estimated by the Inversion	From Directivity Parameters (see table)
L'Aquila	1.444900 km/s	1.2 km/s
Amatrice	1.093450 km/s	1.2 km/s
Visso	1.592550 km/s	1.5 km/s
Norcia	1.102600 km/s	1.3 km/s

Main	Mw	FcMin	FcMax	FactFc	DsMin	DsMax	FactDs
AQU	6.10	0.132	0.376	2.8	1.15	26.7	23.2
AMA	5.97	0.116	0.396	3.4	0.50	19.9	39.8
VIS	5.87	0.100	0.471	4.7	0.23	23.7	103.0
NOR	6.33	0.099	0.254	2.6	1.08	18.2	16.8